Received: 23 September 2022 | Accepted: 1 December 2022

DOI: 10.1002/pamm.202200027

FEM-Modeling of thermal and viscous effects in piezoelectric MEMS loudspeakers

Hamideh Hassanpour Guilvaiee[1,*], **Florian Toth**[1], and **Manfred Kaltenbacher**[2]

[1] TUWien, Vienna, Austria

[2] TUGraz, Graz, Austria

Loudspeakers based on piezoelectric micro-electro-mechanical system (PMEMS) are attracting an increasing interest due to their small size, low electronic power consumption, and easy assembly. These aspects are particularly advantageous in applications like earphones, mobile phones, and in-ear hearing aid devices. However, creating sufficiently high sound pressure levels challenges many existing MEMS loudspeakers. Furthermore, their small dimensions require the consideration of additional physical phenomena like thermoviscous losses, which are often negligible in large loudspeakers. We model and characterize a 3D piezoelectric MEMS loudspeaker in this work using our open-source finite element method (FEM) program openCFS. We use the linearized conservation of mass, momentum, and energy (thermoviscous acoustic PDEs) for a compressible Newtonian fluid (air) and describe the linear elastic solid using the linearized balance of momentum. The coupling between flow and solid fields is then applied using a non-conforming FEM formulation. The standard acoustic partial differential equation (PDE) is used in the far-field, where the thermal and viscous effects are negligible. We study the viscous effects on the displacement and the sound pressure levels (SPLs) of the loudspeaker by parameter studies. These results indicate that at a distance of 13 mm, an SPL of $55\,\mathrm{dB}$ at $5\,\mathrm{kHz}$ is achieved by a single PMEMS loudspeaker with a footprint of $1.7\times1.7\,\mathrm{mm}^2$ under a low driving voltage of only $1\,\mathrm{V}$, which is promising considering its dimensions.

1 Introduction

A PMEMS loudspeaker consists of a piezoelectric actuation mechanism, a membrane (cantilever), and an air chamber. The cantilever is excited by a piezoelectric layer sandwiched between two electrodes bonded to a silicon substrate. Due to their small size, the viscous boundary layer is in the same order of magnitude as the characteristic length; therefore, the thermoviscous effects have to be considered. To model these effects, various methods are proposed: impedance-like boundary condition [1, 2] and low reduced frequency models [3, 4]. However, these models have geometry restrictions. The former is suggested for cases where the viscous boundary layer thickness is sufficiently small compared to the characterized length of the investigated geometry. The latter is suitable for cases where the acoustic wavelength is larger than the geometry length scale. Furthermore, one can use the linearized conservation of mass, momentum and energy to model the thermoviscous effects. Although this method is computationally demanding, it does not have constraints with respect to the geometry [3, 5, 6].

The acoustic behavior of the MEMS loudspeakers depends on the solid structure, its material behavior and acoustic design [7]. To design and characterize PMEMS, various methods such as FEM and lumped element modeling are often applied [8, 9]. Using low reduced frequency, Naderyan et al, [10] suggested an analytical solutions for modeling the thermoviscous damping in perforated MEMS. Their work showed good agreements with FEM model. Based on lumped and FEM models, Liechti et al. developed a model for predicting the viscous losses between the frame and the plate in PMEMS [11].

In this work, we model a 3D PMEMS loudspeaker using our open source FEM program openCFS [12], where thermoviscous effects are taken into account. The device is simulated in two configurations, closed and open back-volume where in the latter, the back and front volumes are connected. Then, PMEMS cantilever displacements are compared in these cases, and the SPL of the device is studied. Finally, the cantilever's displacement and PMEMS resonance frequencies are studied under various atmospheric pressure.

2 Governing Equations

Modeling a PMEMS loudspeaker requires simulating various domains including solid Ω_s, piezoelectric Ω_p, thermoviscous acoustics Ω_tv and acoustic Ω_a. Figure 1 shows an exemplary sketch of these fields and their interfaces. The conservation of energy and the viscous stress tensor should be included to model the thermal and viscous effects in air, especially in small dimensions. In this work, we stick to harmonic analysis, where the assumption of small perturbation around a reference state is acceptable. This assumption allows us to use linearized constitutive laws. The perturbation ansatz is applied to the conservation of mass, momentum, and energy for the pressure p, the density ρ, the temperature T and the velocity $\boldsymbol{v}$ to split

* Corresponding author: e-mail hamideh.hassanpour@tuwien.ac.at

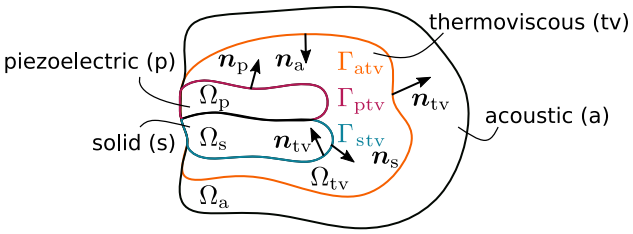

Fig. 1 Simple sketch of a piezoelectric MEMS loudspeaker problem with structure s, piezoelectric p, thermoviscous acoustics tv and acoustic a domains. Where Ω, Γ and $\boldsymbol{n}$ show the domains, interfaces and normal directions.

the total quantities $\bar{(.)}$ into a background $(.)_0$ and (acoustic) perturbation part, i.e.

$$\bar{p} = p_0 + p(\boldsymbol{x}, t)\,, \qquad \bar{\rho} = \rho_0 + \rho(\boldsymbol{x}, t)\,,$$
$$\bar{T} = T_0 + T(\boldsymbol{x}, t)\,, \qquad \bar{\boldsymbol{v}} = \boldsymbol{v}_0 + \boldsymbol{v}(\boldsymbol{x}, t)\,.$$

We solve for the acoustic perturbation quantities, and assume temporally constant background quantities. By assuming air as an isotropic Newtonian fluid, the viscous stress tensor is linear proportional to the strain rate

$$\bar{\boldsymbol{\tau}} = 2\mu\dot{\boldsymbol{s}}_\mathrm{d} + \mu_\mathrm{B}\dot{\boldsymbol{s}}_\mathrm{v}, \tag{1}$$

where μ_B is the second viscosity and μ is the dynamic viscosity. The deviatoric $\dot{\boldsymbol{s}}_\mathrm{d}$ and the volumetric $\dot{\boldsymbol{s}}_\mathrm{v}$ parts of the strain rate tensor are defined by

$$\dot{\boldsymbol{s}}_\mathrm{d} = \dot{\boldsymbol{s}} - \frac{1}{3}\dot{\boldsymbol{s}}_\mathrm{v}\,, \quad \dot{\boldsymbol{s}}_\mathrm{v} = \nabla\cdot\bar{\boldsymbol{v}}\boldsymbol{I}\,, \quad \text{and} \quad \dot{\boldsymbol{s}} = \frac{1}{2}(\boldsymbol{\nabla}\bar{\boldsymbol{v}} + (\boldsymbol{\nabla}\bar{\boldsymbol{v}})^T)\,, \tag{2}$$

where $\dot{\boldsymbol{s}}$ is the total strain rate tensor. The distortion is measured by the deviatoric strain rate, which is the difference between the total and mean volumetric strain rates. Deviatoric strain rate tensor expresses all the deformation rates that cause a shape change without changing the volume. The final definition for the viscous stress tensor is obtained by substituting the strain tensors (2) into the fluid viscous stress tensor expression (1)

$$\bar{\boldsymbol{\tau}} = \mu(\boldsymbol{\nabla}\bar{\boldsymbol{v}} + (\boldsymbol{\nabla}\bar{\boldsymbol{v}})^T) + (\mu_\mathrm{B} - \frac{2}{3}\mu)(\nabla\cdot\bar{\boldsymbol{v}})\boldsymbol{I}\,. \tag{3}$$

This decomposition of viscosities is widely used in literatures as well [13–15]. The ideal gas relation is used to remove the density degrees of freedom.

Finally, the linearized conservation equations are obtained by inserting the perturbation ansatz into the conservation equations and ignoring all nonlinear terms. We also assume the source terms in heat and momentum equations to be zero ($\boldsymbol{v}_0 = 0$). For an ideal gas with no background flow, we arrive at

$$\frac{1}{p_0}\frac{\partial p}{\partial t} + \boldsymbol{\nabla}\cdot\boldsymbol{v} - \frac{1}{T_0}\frac{\partial T}{\partial t} = 0 \quad \text{in } \Omega_\mathrm{tv}\,, \tag{4a}$$
$$\rho_0\frac{\partial \boldsymbol{v}}{\partial t} - \boldsymbol{\nabla}\cdot\boldsymbol{\sigma} = \boldsymbol{0} \quad \text{in } \Omega_\mathrm{tv}\,, \tag{4b}$$
$$\rho_0 c_\mathrm{p}\frac{\partial T}{\partial t} + \boldsymbol{\nabla}\cdot\boldsymbol{q} - \frac{\partial p}{\partial t} = 0 \quad \text{in } \Omega_\mathrm{tv}\,, \tag{4c}$$

where, the fluid stress tensor is $\bar{\boldsymbol{\sigma}} = -\bar{p}\boldsymbol{I} + \bar{\boldsymbol{\tau}}$. The heat flux is expressed by Fourier's law $\boldsymbol{q} = -\gamma_\mathrm{T}\boldsymbol{\nabla}\bar{T}$, where γ_T is the heat conductivity of the fluid.

The acoustic wave equation can be used to model the air behavior where the viscous boundary layers can be neglected. In this case, viscous and thermal dissipation is ignored. This relation is as

$$\frac{1}{c^2}\frac{\partial^2 p_\mathrm{a}}{\partial t^2} - \boldsymbol{\nabla}\cdot\boldsymbol{\nabla}p_\mathrm{a} = 0 \quad \text{in } \Omega_\mathrm{a}\,, \tag{5}$$

where c is the isentropic speed of sound in air.

PMEMS devices contain the flexible solid domain, which is modeled using the conservation of momentum

$$\frac{\partial^2 \rho_i \boldsymbol{u}}{\partial t^2} - \boldsymbol{\nabla}\cdot\boldsymbol{\sigma}_i = \boldsymbol{0} \quad i \in \{\mathrm{s}, \mathrm{p}\} \quad \text{and} \quad \text{in } \Omega_\mathrm{s}\cup\Omega_\mathrm{p}\,, \tag{6}$$

where $\boldsymbol{u}$ denotes the displacement, ρ_i the density of the solid/piezoelectric material, and $\boldsymbol{\sigma}_i$ is the stress tensor. We consider the material behavior in the structure domain as linear elastic but anisotropic, relating stress and strain tensor through the material stiffness tensor $\boldsymbol{C}$ by

$$\boldsymbol{\sigma}_\mathrm{s} = \boldsymbol{C} : \boldsymbol{s} \quad \text{in } \Omega_\mathrm{s}\,, \tag{7}$$

where the solid strain $\boldsymbol{s}$ is defined as $\boldsymbol{s} = \frac{1}{2}\left(\boldsymbol{\nabla u} + (\boldsymbol{\nabla u})^T\right)$. In the piezoelectric domain, the linearized piezoelectric constitutive law is used

$$\boldsymbol{\sigma}_\mathrm{p} = \boldsymbol{C} : \boldsymbol{s} - \boldsymbol{e} \cdot \boldsymbol{E} \quad \text{and} \quad \boldsymbol{D} = \boldsymbol{e} : \boldsymbol{s} + \boldsymbol{\epsilon} \cdot \boldsymbol{E} \quad \text{in } \Omega_\mathrm{p}\,, \tag{8}$$

where $\boldsymbol{e}$ denotes the piezoelectric coupling tensor, $\boldsymbol{E}$ and $\boldsymbol{D}$ are the electric field and flux vectors, respectively, and $\boldsymbol{\epsilon}$ is the electric permittivity tensor. Furthermore, we use Gauss' law to describe the electric flux density by

$$\boldsymbol{\nabla} \cdot \boldsymbol{D} = 0 \quad \text{in } \Omega_\mathrm{p}, \tag{9}$$

and describe the electric field as $\boldsymbol{E} = -\boldsymbol{\nabla}\phi$, where ϕ is the electric scalar potential. This identically fulfills the Faraday's law for the electrostatic case, $\boldsymbol{\nabla} \times \boldsymbol{E} = \boldsymbol{0}$. The final linear formulation for piezoelectricity is obtained by inserting (8) into (6) and (9).

Thermoviscous acoustic domains surround the flexible solid regions. To couple these domains, the following coupling conditions are applied

$$-\boldsymbol{\sigma} \cdot \boldsymbol{n}_\mathrm{tv} = \boldsymbol{\sigma}_\mathrm{s} \cdot \boldsymbol{n}_\mathrm{s}\,, \qquad \frac{\partial \boldsymbol{u}}{\partial t} = \boldsymbol{v}\,, \quad \text{on } \Gamma_\mathrm{stv}\,.$$

These equations enforce the traction continuity and the velocity continuity on the solid-thermoviscous acoustic interface Γ_stv. At the interface between the thermoviscous and the acoustic domain, the following coupling conditions are considered

$$\boldsymbol{\sigma} \cdot \boldsymbol{n} = -p_\mathrm{a}\boldsymbol{n} = \boldsymbol{\sigma}_\mathrm{a} \cdot \boldsymbol{n}\,, \qquad \boldsymbol{v} \cdot \boldsymbol{n} = \boldsymbol{v}_\mathrm{a} \cdot \boldsymbol{n} \quad \text{on } \Gamma_\mathrm{atv}\,,$$

i.e., we apply the traction continuity and the normal velocity continuity on the acoustic and thermoviscous acoustic interface Γ_atv.

3 Finite element formulation

The coupling between the solid and thermoviscous domains are enforced using non-conforming interfaces [6]. The coupling between thermoviscous and acoustics are applied using Nitsche-type mortaring method [16]. These methods apply the interface conditions in the weak sense; therefore, the non-conforming grids are supported on their interfaces. Using these methods, the final FEM formulation for modeling PMEMS is obtained by multiplying the described formulations by appropriate test functions denoted by $()'$ and integrating over the whole computational domains

$$\int_{\Omega_\mathrm{tv}} \frac{1}{p_0} p' \frac{\partial p}{\partial t}\,\mathrm{d}\Omega + \int_{\Omega_\mathrm{tv}} p' \boldsymbol{\nabla} \cdot \boldsymbol{v}\,\mathrm{d}\Omega - \int_{\Omega_\mathrm{tv}} \frac{1}{T_0} p' \frac{\partial T}{\partial t}\,\mathrm{d}\Omega = 0\,, \tag{10a}$$

$$\int_{\Omega_\mathrm{tv}} \rho_0 c_\mathrm{p} T' \frac{\partial T}{\partial t}\,\mathrm{d}\Omega + \int_{\Omega_\mathrm{tv}} \gamma_\mathrm{T} \boldsymbol{\nabla} T' \cdot \boldsymbol{\nabla} T\,\mathrm{d}\Omega - \int_{\Omega_\mathrm{tv}} T' \frac{\partial p}{\partial t}\,\mathrm{d}\Omega + \int_{\Gamma_\mathrm{tv}} T' \boldsymbol{q} \cdot \boldsymbol{n}_\mathrm{tv}\,\mathrm{d}\Gamma = 0\,, \tag{10b}$$

$$\begin{aligned}\int_{\Omega_\mathrm{tv}} \rho_0 \boldsymbol{v}' \cdot \frac{\partial \boldsymbol{v}}{\partial t}\,\mathrm{d}\Omega + \int_{\Omega_\mathrm{tv}} \boldsymbol{\nabla} \boldsymbol{v}' : \boldsymbol{\sigma}_\mathrm{tv}\,\mathrm{d}\Omega + \int_{\Gamma_\mathrm{tv}} \boldsymbol{v}' \cdot \boldsymbol{\sigma} \cdot \boldsymbol{n}\,\mathrm{d}\Gamma + \int_{\Gamma_\mathrm{tva}} \boldsymbol{v}' \cdot \boldsymbol{n} p_\mathrm{a}\,\mathrm{d}\Gamma \\ + \int_{\Gamma_\mathrm{vs}} \boldsymbol{v}' \cdot \boldsymbol{\sigma}_\mathrm{s} \cdot \boldsymbol{n}\,\mathrm{d}\Gamma - \beta \frac{p_\mathrm{e}^2}{h_\mathrm{e}} \int_{\Gamma_\mathrm{vs}} \boldsymbol{v}' \cdot \left(\frac{\partial \boldsymbol{u}}{\partial t} - \boldsymbol{v}\right)\mathrm{d}\Gamma = \boldsymbol{0}\,,\end{aligned} \tag{10c}$$

$$\int_{\Omega_\mathrm{a}} \frac{1}{c^2} p_\mathrm{a}' \frac{\partial^2 p_\mathrm{a}}{\partial t^2}\,\mathrm{d}\Omega + \int_{\Omega_\mathrm{a}} \boldsymbol{\nabla} p_\mathrm{a}' \cdot \boldsymbol{\nabla} p_\mathrm{a}\,\mathrm{d}\Omega - \int_{\Gamma_\mathrm{atv}} \rho_0\, p_\mathrm{a}' \frac{\partial \boldsymbol{v}}{\partial t} \cdot \boldsymbol{n}\,\mathrm{d}\Gamma = 0\,, \tag{10d}$$

$$\begin{aligned}\int_{\Omega_\mathrm{s} \cup \Omega_\mathrm{p}} \boldsymbol{u'} \cdot \rho_i \frac{\partial^2 \boldsymbol{u}}{\partial t^2}\Omega + \int_{\Omega_\mathrm{s} \cup \Omega_\mathrm{p}} \boldsymbol{\nabla u}' : \boldsymbol{C} : \boldsymbol{s}\,\mathrm{d}\Omega + \int_{\Omega_\mathrm{p}} \boldsymbol{\nabla u}' : \boldsymbol{e} \cdot \nabla\phi\,\mathrm{d}\Omega - \int_{\Gamma_\mathrm{s} \cup \Gamma_\mathrm{p}} \boldsymbol{u}' \cdot \boldsymbol{\sigma}_\mathrm{s} \cdot \boldsymbol{n}\,\mathrm{d}\Gamma \\ - \int_{\Gamma_\mathrm{stv}} \boldsymbol{u}' \cdot \boldsymbol{\sigma}_\mathrm{s} \cdot \boldsymbol{n}\,\mathrm{d}\Gamma + \beta \frac{p_\mathrm{e}^2}{h_\mathrm{e}} \int_{\Gamma_\mathrm{stv}} \boldsymbol{u}' \cdot \left(\frac{\partial \boldsymbol{u}}{\partial t} - \boldsymbol{v}\right)\mathrm{d}\Gamma = \boldsymbol{0},\end{aligned} \tag{10e}$$

$$- \int_{\Omega_\mathrm{p}} \boldsymbol{\nabla}\phi' \cdot \boldsymbol{e} : \boldsymbol{s}\,\mathrm{d}\Omega + \int_{\Omega_\mathrm{p}} \boldsymbol{\nabla}\phi' \cdot \boldsymbol{\epsilon} \cdot \boldsymbol{\nabla}\phi\,\mathrm{d}\Omega = 0. \tag{10f}$$

Equations (10a), (10b) and (10c) are the weak form of conservation of mass, energy and momentum for the thermoviscous domain which includes coupling with acoustic and solid domains. Equations (10d), (10e) and (10f) are the weak form of the acoustic wave equation, flexible solid and piezoelectric Gauss formulation. On the walls, we enforce the homogeneous Dirichlet boundary condition. This means applying $\boldsymbol{u} = 0$ and $\boldsymbol{v} = 0$ on the solid and thermoviscous acoustic boundaries, respectively.

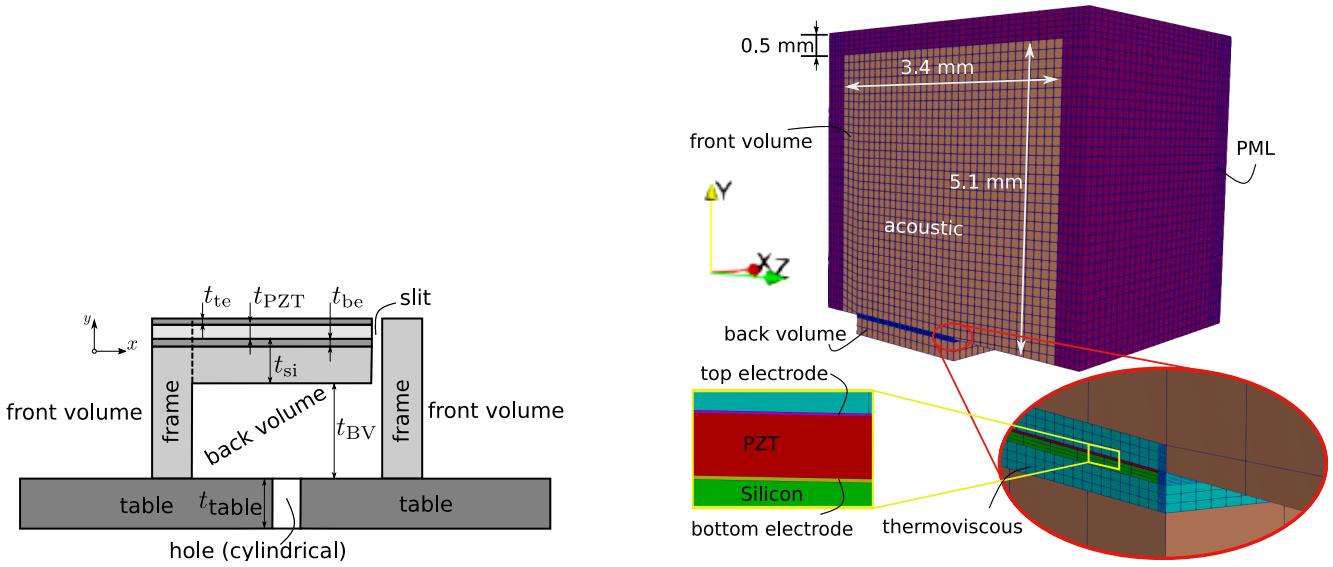

(a) Simple sketch of PMEMS. Different layers of the solid structure are displayed (dimensions are not to scale).

(b) Mesh discretization of PMEMS in closed back-volume configuration. Non-conforming mesh discretizations are used on the interfaces.

Fig. 2: PMEMS loudspeaker

Table 1: PMEMS loudspeaker layers

Layer	Silicon (Si)	Top electrode (te)	Bottom electrode (be)	PZT
Thickness in µm	9.1	0.1	0.13	2.1
Density ρ in $\mathrm{kg\,m^{-3}}$	2330	21450	7700	7600
Young's Modulus E in Pa	$1.12{\cdot}10^{11}$	$1.68{\cdot}10^{11}$	$9.8{\cdot}10^{10}$	$1.2{\cdot}10^{11}$
Poisson's ratio ν	0.28	0.38	0.23	0.33

Table 2: Piezoelectric material properties

Property		Value
Permittivity $\boldsymbol{\epsilon}$	$\epsilon_{11} = \epsilon_{22}$	$2.771{\cdot}10^{-8}$
in $\mathrm{As/Vm}$	ϵ_{33}	$3.010{\cdot}10^{-8}$
Piezoelectric coupling	$e_{31} = e_{32}$	-3.88
tensor e in $\mathrm{A\,s\,m^{-2}}$	$e_{24} = e_{15} = e_{33}$	7.76

Table 3: Additional dimensions (values in µm)

Property	values in µm
t_{BV}	280
t_{table}	2000
l_s	1700
w_s	1700

4 Numerical simulation and results

Using the described formulation, we model and characterize a PMEMS loudspeaker. This loudspeaker is modeled in two configurations: closed and open back-volume. Figure 2(a) shows the composition of this model including cantilever's multiple layers, acoustic domains and the cylindrical hole with $1\,\mathrm{mm}$ diameter. The closed or open cylindrical hole separates or connects the back and front volumes and creates the closed back-volume and open back-volume configurations, respectively. This connection leads to complete different behaviors of the studied PMEMS due to the damping and viscous forces. The studied PMEMS contains four flexible solid layers showed in Fig. 2(a). The material parameters and thickness of these layers are given in tables 1 and 3. In these tables, t_{BV}, l_s and w_s are the thickness of back-volume, the length and the width of solid layers. Air material properties such as density, visosity and etc. at room temperature and under atmopheric pressure of $1\,\mathrm{bar}$ are illustrated in [16].

Changing the atmospheric pressure affects air behavior. Density and compression modulus are air material properties that vary with different pressures. The relation between air density and pressure is described using the ideal gas relation as $\rho = \frac{p}{RT}$, where R is the gas constant. Accordingly, the air compression modulus K varies for different pressure as $K = \kappa p_0$, where κ is the adiabatic exponent. Other air properties do not vary in different reference pressures. The air viscosity varies at different temperatures; however, under different pressures at room temperature, it stays almost constant [17].

Figure 2(b) depicts the mesh discretization used for modeling the device in the closed back-volume configuration. In the open back-volume, the same geometry is modeled by using a larger acoustic domain, and considering the table (where the device is placed) and frame structures. Since these structures are assumed as perfectly rigid bodies, one can eliminate them from the geometry. The non-conforming interfaces are used among the solid-thermoviscous acoustic and acoustic-thermoviscous acoustic interfaces.

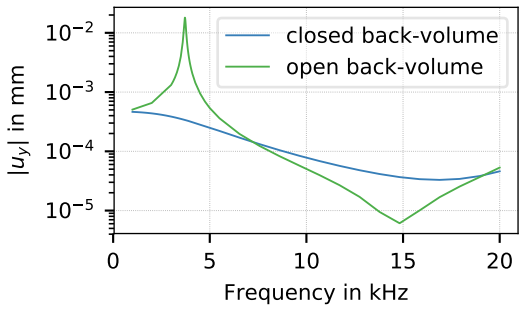

Fig. 3: Maximum displacement of PMEMS in closed and open back-volume configurations with excitation of 1 V at 1 bar

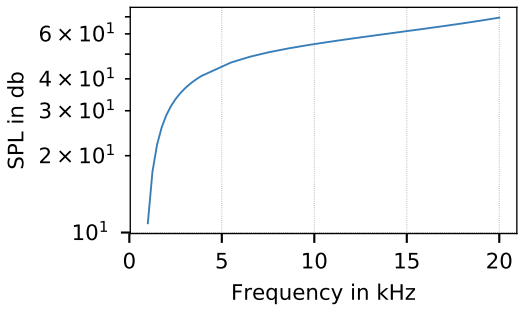

Fig. 4: Sound pressure level (SPL) at distance 13 mm in closed back-volume configuration with excitation of 1 V under 1 bar.

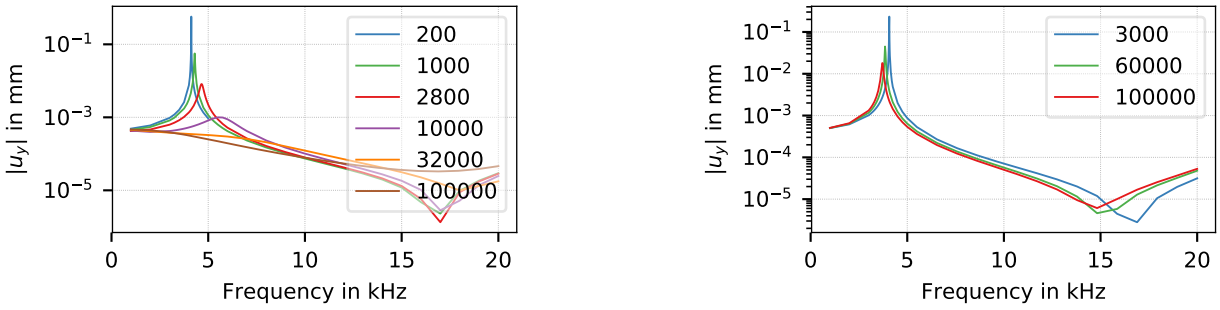

(a) Closed back-volume

(b) Open back-volume

Fig. 5: PMEMS maximum cantilever's displacement under various atmospheric pressure with excitation of 1 V under 1 bar

Figure 3 shows the maximum displacement of the PMEMS cantilever over frequency range of 1 to 20 kHz with the excitation of 1 V, under the atmospheric pressure of 1 bar. In the closed back-volume, the first resonance frequency of the device ($\sim$4 kHz) is completely damped; however, the displacement shows the first resonance in the open back-volume. The damping forces are originated from two sources: viscous and pressure forces. In the closed back-volume case, the air is forced to move thorough the narrow slit by cantilever displacement, which causes higher viscous damping. On the contrary, in the open back volume this damping is negligible.

We further studied the SPL at the distance of 13 mm in the closed back-volume configuration with the excitation of 1 V under the atmospheric pressure of 1 bar. The PMEMS produces an SPL of 55 dB at the frequency of the 5 kHz, which is promising considering the loudspeaker's small dimensions. In the range of 3 to 20 kHz, the SPL responses are relatively flat.

PMEMS device is further studied in various atmospheric pressures. Figure 5 shows the maximum displacement of PMEMS cantilever over frequency in open and closed back-volume configurations. At lower frequencies, the closed back-volume system shows sharper peaks with higher amplitudes. Increasing atmospheric pressure from 200 to 100 000 Pa causes higher viscous damping and additional pressure forces resulting in lower cantilever amplitudes. These higher forces also leads to higher cantilever stiffness which shifts the resonances to the higher frequencies (Fig. 5(a)). In the open back-volume (Fig. 5(b)), the viscous and pressure effects are much lower than in the closed back-volume configuration due to the connection of the front and back volumes. Thus, we observe the resonance of $\sim$4 kHz for various atmospheric pressures from 3000 to 100 000 Pa. Similar to the closed back-volume, displacement amplitudes are higher with sharper peaks in lower atmospheric pressure. On the contrary, the resonances are slightly shifted to lower frequencies under higher atmospheric pressures. Increasing pressure results in an increase in air density, which causes lower resonances, due to the increased added-mass effect.

5 Conclusion

In this work, we first presented a finite element formulation for modeling thermoviscous effects in the acoustic domains. Further, we add a non-conforming finite element formulation for coupling this domain to solid and acoustic domains. Using these formulations, we have modeled a 3D PMEMS loudspeaker in closed and open back-volume configurations. In the closed back-volume configuration, the air is forced to move thorough the narrow slit by cantilever displacement. This caused high damping effects which faded out the first resonance frequency. These effects are not as pronounced in the open back-volume as in the closed back-volume; therefore, the system still demonstrates its resonance frequency at $\sim$4 kHz. Furthermore, atmospheric pressure was changed from 200 to 100 000 Pa. This affected the viscous and pressure forces and, therefore, the displacement amplitudes and resonance frequencies. In both configurations, lower pressures caused lower damping and

subsequently higher displacement amplitudes and sharper peaks. In the closed back-volume, the resonances were shifted to higher frequencies with higher atmospheric pressures. These higher resonances resulted from the increased stiffness of PMEMS' cantilever due to the higher pressure forces. In the open back-volume, this force was negligible; therefore, higher pressures caused higher densities and lower resonances.

Acknowledgements This work was partly funded by the Austrian Research Promotion Agency (FFG) within the program line "Bridge" (project number 868033). The authors acknowledge TU Wien Bibliothek for financial support through its Open Access Funding Programme.

References

[1] R Bossart, N Joly, and M Bruneau. Hybrid numerical and analytical solutions for acoustic boundary problems in thermo-viscous fluids. *Journal of Sound and Vibration*, 263(1):69–84, 2003.

[2] Martin Berggren, Anders Bernland, and Daniel Noreland. Acoustic boundary layers as boundary conditions. *Journal of Computational Physics*, 371:633–650, 2018.

[3] Willem Marinus Beltman. Viscothermal wave propagation including acousto-elastic interaction, part I: theory. *Journal of Sound and Vibration*, 227(3):555–586, 1999.

[4] Marten Jozef Johannes Nijhof. *Viscothermal wave propagation*. PhD thesis, Universiteit Twente, 2010.

[5] W R Kampinga, Y H Wijnant, and André de Boer. An efficient finite element model for viscothermal acoustics. *Acta Acustica united with Acustica*, 97(4):618–631, 2011.

[6] Hamideh Hassanpour Guilvaiee, Florian Toth, and Manfred Kaltenbacher. A Non-conforming Finite Element Formulation for Modeling Compressible Viscous Fluid and Flexible Solid Interaction. *International Journal for Numerical Methods in Engineering*, 0(July):1–21, 2022.

[7] Haoran Wang, Yifei Ma, Qincheng Zheng, Ke Cao, Yao Lu, and Huikai Xie. Review of recent development of MEMS speakers. *Micromachines*, 12(10), 2021.

[8] Ki Hong Park, Zhi Xiong Jiang, and Sang Moon Hwang. Design and analysis of a novel microspeaker with enhanced low-frequency spl and size reduction. *Applied Sciences (Switzerland)*, 10(24):1–17, 2020.

[9] Wei Liu, Jie Huang, Yong Shen, and Jiazheng Cheng. Theoretical modeling of piezoelectric cantilever MEMS loudspeakers. *Applied Sciences (Switzerland)*, 11(14), 2021.

[10] Vahid Naderyan, Richard Raspet, and Craig Hickey. Thermo-viscous acoustic modeling of perforated micro-electro-mechanical systems (MEMS). *The Journal of the Acoustical Society of America*, 148(4):2376–2385, 2020.

[11] Romain Liechti, Stephane Durand, Thierry Hilt, Fabrice Casset, Christel Dieppedale, Thierry Verdot, and Mikael Colin. A Piezoelectric MEMS Loudspeaker Lumped and FEM models. *2021 22nd International Conference on Thermal, Mechanical and Multi-Physics Simulation and Experiments in Microelectronics and Microsystems, EuroSimE 2021*, 2021.

[12] Manfred Kaltenbacher, Florian Toth, and Hamideh Hassanpour. openCFS.

[13] L. D. Landau and E. M. Lifshitz. *Fluid mechanics. 2nd Edition. Course of theoretical physics. Volume 6.* Pergamon press, 1987.

[14] Peter Barkholt Muller and Henrik Bruus. Numerical study of thermoviscous effects in ultrasound-induced acoustic streaming in microchannels. *Physical Review E*, 90(4):43016, 2014.

[15] Jonas Helboe Joergensen and Henrik Bruus. Theory of pressure acoustics with thermoviscous boundary layers and streaming in elastic cavities. *The Journal of the Acoustical Society of America*, 149(5):3599–3610, 2021.

[16] Florian Toth, Hamideh Hassanpour Guilvaiee, and Georg Jank. Acoustics on small scales: Modelling viscous effects in MEMS devices. *Elektrotechnik und Informationstechnik*, 2021.

[17] A. D'Angola, G. Colonna, C. Gorse, and M. Capitelli. Thermodynamic and transport properties in equilibrium air plasmas in a wide pressure and temperature range. *European Physical Journal D*, 46(1):129–150, 2008.

